PAPER

Interstitial fluid pressure regulates collective invasion in engineered human breast tumors *via* Snail, vimentin, and E-cadherin†

Alexandra S. Piotrowski-Daspit,[a] Joe Tien[bc] and Celeste M. Nelson*[ad]

Many solid tumors exhibit elevated interstitial fluid pressure (IFP). This elevated pressure within the core of the tumor results in outward flow of interstitial fluid to the tumor periphery. We previously found that the directionality of IFP gradients modulates collective invasion from the surface of patterned three-dimensional (3D) aggregates of MDA-MB-231 human breast cancer cells. Here, we used this 3D engineered tumor model to investigate the molecular mechanisms underlying IFP-induced changes in invasive phenotype. We found that IFP alters the expression of genes associated with epithelial–mesenchymal transition (EMT). Specifically, the levels of Snail, vimentin, and E-cadherin were increased under pressure conditions that promoted collective invasion. These changes in gene expression were sufficient to direct collective invasion in response to IFP. Furthermore, we found that IFP modulates the motility and persistence of individual cells within the aggregates, which are also influenced by the expression levels of EMT markers. Together, these data provide insight into the molecular mechanisms that guide collective invasion from primary tumors in response to IFP.

Insight, innovation, integration

High IFP, a characteristic of most solid tumors, has been shown to influence the migratory behavior of cancer cells in a variety of 3D culture models. However, the underlying mechanisms remain elusive. Here, we used a 3D microfluidic flow chamber to control IFP across cancer cell aggregates and investigated how pressure-induced changes in gene expression regulate collective invasion and individual cell motility. We show that IFP dramatically alters gene expression, and that these changes are both necessary and sufficient to determine the invasive phenotype. This study integrates an innovative engineered tumor, analytical methodologies, and genetic manipulation, to provide new insight into the mechanisms that guide collective invasion of tumor cells in response to IFP.

Introduction

During the transformation of healthy tissue into invasive cancer, the cellular microenvironment undergoes several physical changes.[1] As solid tumors grow, their lymphatic vessels collapse due to increased mechanical compression from the presence of extra cells.[2] The non-functioning intra-tumoral lymphatic system impairs drainage from the tumor, and hyperpermeable blood vessels lead to an accumulation of fluid and plasma macromolecules

within the interstitium.[2] As a result, the interstitial fluid pressure (IFP) within tumors tends to be dramatically elevated, resulting in localized interstitial hypertension.[2,3] In human and animal tumors, IFP rises steeply within the tumor periphery and plateaus at values as high as 50 mm Hg (compared to 0 mm Hg in normal tissue),[4–9] resulting in an outward flow of fluid from the tumor core.[10,11] Cellular responses to this physical abnormality result in increased tumorigenic potential. High IFP has been associated with poor prognosis[12] and increased lymph node metastasis[9] in cervical cancer. The molecular mechanisms underlying the effects of IFP on tumor progression and invasion, however, remain unclear.

Three-dimensional (3D) culture models have recently been used to investigate the effects of elevated IFP, interstitial flow, and mechanical compression on the invasive phenotype of breast cancer cells.[13–17] In one study, a hydrostatic pressure gradient was applied across MDA-MB-231 human breast cancer cells embedded sparsely in an extracellular matrix (ECM) gel.[13]

[a] *Department of Chemical & Biological Engineering, Princeton University, 303 Hoyt Laboratory, William Street, Princeton, NJ 08544, USA. E-mail: celesten@princeton.edu; Fax: +1-609-258-1247; Tel: +1-609-258-8851*

[b] *Department of Biomedical Engineering, Boston University, Boston, MA 02215, USA*

[c] *Division of Materials Science and Engineering, Boston University, Boston, MA 02215, USA*

[d] *Department of Molecular Biology, Princeton University, Princeton, NJ 08544, USA*

† Electronic supplementary information (ESI) available. See DOI: 10.1039/c5ib00282f

Interstitial flow was found to increase the percentage of cells that migrated as well as their speed, suggesting that IFP can enhance tumor invasion.[13] Cells migrated parallel to the direction of fluid flow *via* autologous chemotaxis, a phenomenon that was also observed in 3D Boyden chambers.[18] In a similar study, applying a hydrostatic pressure gradient across a single cell suspension of the same cell line in a type I collagen gel induced the cells to migrate primarily against the direction of flow at higher seeding densities.[14,15] Interstitial flow has also been shown to influence the type of cell motility, promoting amoeboid over mesenchymal migration in MDA-MB-231 cells.[19] Although it is clear that elevated IFP and interstitial flow influence the migration of cancer cells in culture, the underlying molecular mechanisms are unknown.[9]

The specific responses of cancer cells to IFP appear to depend heavily on experimental context. In many solid breast tumors, cells do not exist in isolation; rather, they are packed together, much as in normal tissues. To recapitulate the aggregate nature of cells in a solid tumor, we recently developed an engineered 3D culture model, and used this system to apply a hydrostatic pressure drop across a packed aggregate of MDA-MB-231 human breast cancer cells. This model yields a more physiologically relevant system to study collective cell behavior, such as IFP-induced invasion.[20] We found that cells formed multicellular chains that invaded collectively from the tips of the aggregates. In addition, we found that invasion occurred against the direction of flow.[16] Surprisingly, interstitial hypertension (*i.e.*, elevated IFP at the base of the aggregates relative to the IFP at the tip) inhibited invasion from the tumor margin. Pressure-induced convection of tumor-conditioned medium controlled the invasive phenotype at the margin of the engineered tumors.

Here we took advantage of this 3D engineered tumor model to define the effects of IFP on invasion-related gene expression in human breast and prostate cancer cells, focusing specifically on genes associated with epithelial–mesenchymal transition (EMT).[21] Using quantitative RT-PCR, we measured the relative transcript levels of several genes under three pressure profiles: control (*i.e.*, uniform IFP), interstitial hypertension, and interstitial hypotension (elevated IFP at the tip of the aggregates relative to the base). We found that interstitial hypertension inhibited invasion and decreased expression of both mesenchymal and epithelial markers. Conversely, interstitial hypotension promoted invasion in part by increasing expression of the mesenchymal genes vimentin and Snail. Surprisingly, interstitial hypotension also increased the expression of epithelial markers E-cadherin and keratin-8. Using overexpression and RNAi strategies, we found that IFP-induced changes in gene expression were required to produce the observed invasive phenotype. Finally, we found that individual cells in aggregates under non-uniform IFP were more motile than those under uniform IFP, and that these characteristics were also modulated by changes in the expression levels of EMT markers. Together, these data highlight the effects of IFP on tumor cell migration and collective invasion in a physiologically relevant 3D culture model, and provide insight into the molecular mechanisms underlying the effects of IFP on invasive phenotype in solid tumors.

Materials and methods

3D engineered tumor model

MDA-MB-231 human breast cancer cells and PC-3 human prostate cancer cells (passed at a 1 : 4 ratio, and used from passage 6–9) were obtained from the American Type Culture Collection and cultured in DMEM/F12 growth medium (Hyclone) or RPMI 1640 growth medium (Hyclone) supplemented with 10% fetal bovine serum (FBS; Atlanta Biologicals) and 50 µg mL^{-1} gentamicin (Gibco), respectively. Engineered tumors consisted of aggregates of MDA-MB-231 or PC-3 cells embedded in collagen gels housed within chambers of polydimethylsiloxane (PDMS), and were fabricated as described previously.[16] Acid-extracted bovine type I collagen (Koken) was neutralized with NaOH to a pH of 8.5–9 and diluted with cell culture medium to a final concentration of 4 mg mL^{-1}. Seeded channels were incubated at 37 °C for two days. To apply a hydrostatic pressure gradient, the heights of medium in the reservoirs adjacent to the channel either on the side of the tumor base (P_{base}) or on the side of the tumor tip (P_{tip}) were altered using PDMS gaskets two days after seeding. The pressure differential $|P_{base} - P_{tip}|$ was ~1.6 cm H$_2$O or ~1.2 mm Hg. Upon establishment of a pressure differential, flow speed in the channels was calculated to be ~1 µm s^{-1}, similar to what has been reported *in vivo*.[22] To establish moderate pressure profiles of either type, $P_{base} \leq P_{tip}$ or $P_{base} \geq P_{tip}$, we added a slight excess of medium to one side such that $|P_{base} - P_{tip}|$ was ~0.2 cm H$_2$O or ~0.15 mm Hg. To maintain the pressure profiles, we replenished the medium twice per day. Samples were maintained in culture for up to nine days. To inhibit matrix degradation, GM6001 (40 µM; Calbiochem) was added to the high-pressure reservoir.

Plasmids, transfection, and adenoviral transduction

The cDNA for human vimentin was PCR-amplified from pENTR-vimentin and ligated into the p3xFlag-CMV vector (Sigma Aldrich) using EcoRI and BamHI restriction sites. Empty p3xFlag-CMV vector was used as a control. Expression plasmids for shRNA against Snail, vimentin, and E-cadherin, pLKO.1-Snail-shRNA (shSnail), pLKO.1-vimentin-shRNA (shVim), and pLKO.1-E-cadherin-shRNA (shEcad), were obtained from Sigma Aldrich (TRCN0000063819, TRCN0000029119, and TRCN0000237840, respectively). The control scrambled shRNA plasmid, pLKO.1-scramble-shRNA (shScr), was obtained from Addgene (plasmid 1864). Ectopic expression of E-cadherin was achieved using pcDNA3.1-E-cadherin-GFP (Addgene; plasmid 28009), with pcDNA3.1-YFP as a control. MDA-MB-231 or PC-3 cells were transiently transfected with mammalian or shRNA expression constructs using Lipofectamine 3000 transfection reagent (Invitrogen). MDA-MB-231 cells stably expressing E-cadherin, shScr, shSnail, shVim, or shEcad were collected from pooled populations that were selected using G418 (1 mg mL^{-1}) or puromycin (1 µg mL^{-1}) for three weeks. Ectopic Snail expression was achieved by transducing cells with an adenoviral vector, AdSnail-GFP,[23] with AdGFP as a control. For live imaging, cells were transduced with AdH2B-mCherry. Cells were transduced at an MOI resulting in >99% transduction efficiency.

For mosaic experiments, aggregates were formed using 30% MDA-MB-231 cells stably expressing YFP or Ecad-GFP and 70% untransduced cells.

Quantitative real-time PCR

Samples were treated with a 2 mg mL^{-1} solution of collagenase A (Sigma Aldrich) in cell culture medium for five minutes prior to isolation of total RNA using the Qiagen RNeasy Mini Kit (Qiagen, Inc.). Isolated RNA was used to synthesize cDNA using a Verso cDNA Synthesis Kit (Thermo Scientific). Transcript levels were measured by quantitative real-time PCR using a BioRad Mini-Opticon instrument and the iTaq Universal SYBR Green Supermix (BioRad). Primers for E-cadherin, keratin-8, vimentin, Snail, and 18S rRNA (Table S1, ESI†) were designed using Beacon Designer software (BioRad) and determined to be specific using BLAST and dissociation curve analysis. All transcript levels were normalized to that of 18S rRNA in the same sample. Experiments were performed independently in triplicate, with six samples per treatment condition per experiment.

Timelapse microscopy

Samples transduced with AdH2B-mCherry were imaged beginning seven days after seeding. Timelapse movies were collected using a Hamamatsu C4742-95 camera attached to a Nikon Ti-U inverted microscope and fitted with a humidified environmental chamber held at 37 °C and 5% CO$_2$. Image stacks (960 μm × 730 μm × 200 μm, spaced 20 μm in the z-direction) were acquired using a Plan Fluor 10×/0.3 NA objective every hour for a total of twenty hours.

Quantitative image analysis

Samples were imaged under phase-contrast microscopy using a 10×/0.4 NA objective on a Nikon Ti-U inverted microscope (Nikon) with a Hamamatsu Orca CCD camera. On days 7–9 after seeding, samples under all pressure conditions were fixed with 4% paraformaldehyde in PBS (added to the well on the higher pressure side for hypertension and hypotension ($P_{\text{base}} \neq P_{\text{tip}}$), or to the well on the P_{base} side for the control pressure condition ($P_{\text{base}} = P_{\text{tip}}$)) and washed three times with PBS. Nuclei were labeled using Hoechst 33342 and visualized under UV illumination. Invasions were defined as multicellular protrusions from the aggregate tips. The lengths of these protrusions and invadopodia (anuclear protrusions) were measured using ImageJ software (NIH). Invadopodial density per aggregate was calculated as total length of invadopodia divided by the perimeter of the aggregate. For analysis of live imaging data, cells within 150 μm of aggregate tips were tracked manually using the MTrackJ plugin in Image J. Cell tracks were exported to Microsoft Excel in order to calculate speed, net displacement, path length, and directionality ratio (net displacement divided by path length of a trajectory) using open-source macros from DiPer.[24] Correlations between individual cell tracks were determined using the sample cross-covariance function as described previously.[25]

Immunofluorescence analysis

Fixed samples were removed from the PDMS chamber, blocked with 10% goat serum and 0.1% Triton X-100, and incubated overnight in primary antibody diluted 1:200 in blocking buffer. Blocked samples were washed with 0.1% Triton X-100 and incubated overnight with Alexa Fluor-conjugated secondary antibody (Invitrogen) diluted 1:1000 in blocking buffer. After additional washing, samples were visualized using a spinning disk confocal (BD Biosciences) attached to a Nikon Ti-U microscope using a Plan Fluor 20×/0.45 NA objective. Primary antibodies were used to detect cortactin (Millipore), Tks5 (M-300; Santa Cruz), phosphorylated FAK (on Y^{397}; Invitrogen), MMP14 (Millipore), and β-catenin (Sigma Aldrich). Isotype control staining was negative.

Immunoblotting

Samples were lysed with RIPA lysis buffer (Thermo Scientific) supplemented with protease inhibitors (Roche), and protein concentrations were measured using the Pierce Bicinchoninic acid (BCA) Protein Assay Kit (Thermo Scientific). Samples were then mixed with Laemmli sample buffer, boiled at 95 °C for 5 min, resolved by SDS-PAGE, and transferred to nitrocellulose membranes, which were blocked in 5% nonfat milk in Tris-buffered saline with Tween 20 (TBST) buffer. Blocked membranes were incubated overnight at 4 °C in blocking buffer containing antibodies specific for vimentin (clone VIM-13.2; Sigma Aldrich), Snail (clone L70G2; Cell Signaling), E-cadherin (clone 24E10; Cell Signaling), or β-actin (Cell Signaling). Signals were visualized using the ECL Plus Western Blotting Detection System (GE Healthcare).

Statistical analysis

Results were analyzed in GraphPad Prism (GraphPad Software). To compare invasion frequencies, we used Fisher's exact test. To compare invadopodial lengths or invadopodial length densities, we used the Mann–Whitney U test. To correlate invadopodial length density with hydrostatic pressure differential, we used Spearman's rank correlation test. To compare relative transcript levels among different pressure conditions, we used ANOVA with Bonferroni's post-test for multiple comparisons. We used the Student's t-test to compare relative transcript levels of transduced cells, percentages of YFP- or GFP-expressing cells forming invasions in mosaic experiments, and sample cross-correlation coefficients. To compare the numbers or total lengths of multicellular invasions for gene manipulation conditions, we used the Chi-Square test and Kruskal–Wallis test with Dunn's multiple comparison post-test, respectively. Mean values represent at least three independent experiments, and error bars represent standard error of the mean. For all statistical tests, $P < 0.05$ was considered to be statistically significant.

Results

Interstitial fluid pressure regulates collective invasion from tumor cell aggregates

We used a 3D microfluidic culture model to engineer intact aggregates of MDA-MB-231 human breast cancer cells embedded within a gel of type I collagen (Fig. 1A). Briefly, a needle was used
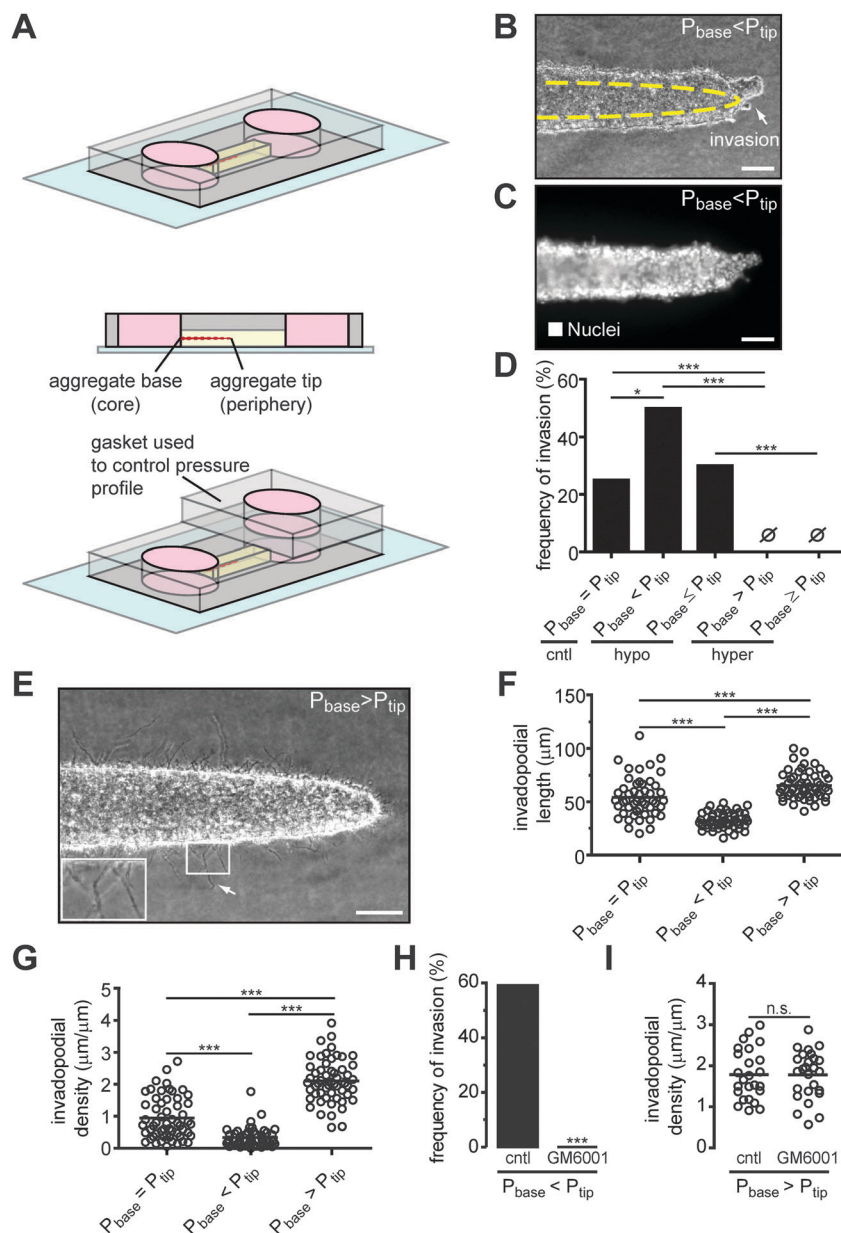
Fig. 1 IFP determines the invasive phenotype of human breast cancer aggregates. (A) Schematic of the 3D culture model. Top panel: perspective view at a control pressure profile. Middle panel: side view. Bottom panel: perspective view showing the use of a gasket to apply a pressure difference. (B) Phase-contrast image of an aggregate under $P_{base} < P_{tip}$. Arrow indicates collective invasion. Dashed yellow line denotes the shape of the aggregate at day 0. (C) Hoechst 33342 staining of cell nuclei (white). (D) Frequency of invasion of aggregates under $P_{base} = P_{tip}$ ($n = 49$), $P_{base} < P_{tip}$ ($n = 50$), or $P_{base} > P_{tip}$ ($n = 51$). (E) Phase-contrast image of an aggregate under $P_{base} > P_{tip}$. Arrow indicates invadopodia. Inset shows magnified image of boxed region. (F) Average length of invadopodia for aggregates under $P_{base} = P_{tip}$ ($n = 49$), $P_{base} < P_{tip}$ ($n = 49$), or $P_{base} > P_{tip}$ ($n = 55$). (G) Invadopodial length density for aggregates under $P_{base} = P_{tip}$ ($n = 57$), $P_{base} < P_{tip}$ ($n = 51$), or $P_{base} > P_{tip}$ ($n = 56$). (H) Frequency of invasion with ($n = 26$) and without ($n = 27$) GM6001 in aggregates under $P_{base} < P_{tip}$. (I) Invadopodial length densities with ($n = 26$) and without ($n = 25$) GM6001 in samples under $P_{base} > P_{tip}$. *$P < 0.05$, ***$P < 0.001$. Scale bars, 100 μm.

to mold a blind-ended channel within the gel, which was filled with a concentrated suspension of cells.[16] This procedure yielded an aggregate of cells, the base of which mimicked the core of a solid tumor while the tip mimicked the tumor periphery. Tumor aggregates were subjected to different hydrostatic pressure profiles by independently varying the pressure at the base of the aggregate (P_{base}) from that at the tip (P_{tip}). This system allowed us to determine the effects of IFP on

collective invasion. Invasions were defined as multicellular protrusions emanating from aggregate tips (Fig. 1B), as determined using a nuclear stain (Fig. 1C). The characteristically collective invasions that we observed are consistent with reports by others using the same cell line.[26,27]

Under the control pressure profile ($P_{base} = P_{tip}$), 25% of aggregates developed invasions (Fig. 1D). Under $P_{base} > P_{tip}$, which mimics the interstitial hypertension frequently observed

in solid tumors, invasions were absent (0 out of 51 samples). In contrast, when aggregates were subjected to interstitial hypotension ($P_{base} < P_{tip}$), 50% developed invasions. Even moderate pressure profiles of either type ($P_{base} \geq P_{tip}$ or $P_{base} \leq P_{tip}$) affected invasion frequency. IFP similarly controlled invasion from aggregates of PC-3 prostate cancer cells (Fig. S1A, ESI†). These data suggest that interstitial hypertension prevents invasion, whereas interstitial hypotension promotes invasion. Cells thus invaded collectively primarily against the direction of fluid flow, which is consistent with what others have reported for densely seeded single-cell suspensions of MDA-MB-231 cells.[14,15]

Although it prevented invasion, interstitial hypertension induced the formation of anuclear membrane protrusions (Fig. 1E) that resembled invadopodia, membrane protrusions of tumor cells that locally degrade the ECM.[28] We quantified the response of these putative invadopodia to IFP by measuring their average length and density. Aggregates under hypertension displayed longer and denser invadopodia than those under control pressure or hypotension (Fig. 1F and G). Similar results were observed in samples under moderate hypertension or hypotension (Fig. S1B, ESI†). The density of putative invadopodia did not correlate with the magnitude of the pressure profile for interstitial hypertension (Fig. S1C, ESI†).

The formation of invadopodia is believed to precede invasion by tumor cells.[29] We therefore sought to determine whether the membrane protrusions observed in our samples primarily under hypertension displayed characteristic features of invadopodia, such as the ability to degrade the ECM. We treated samples with the broad-spectrum matrix metalloproteinase (MMP) inhibitor, GM6001, which prevented invasion under hypotension (Fig. 1H), suggesting that matrix remodeling is required for collective invasion. Treatment with GM6001 did not, however, suppress the formation of putative invadopodia under hypertension (Fig. 1I). We also stained samples for the invadopodial markers cortactin, Tks5, phosphorylated FAK (pY[397]),[30] and MMP14. The multicellular collective invasions that formed under hypotension strongly expressed these markers (Fig. S2, ESI†). The putative invadopodia in samples under hypertension were enriched in cortactin and Tks5. Staining for MMP14 was weak, consistent with the behavior of GM6001-treated samples (Fig. S2, ESI†). The levels of phosphorylated FAK in the putative invadopodia were also weak. These results suggest that the anuclear membrane protrusions observed in the tumor aggregates are non-functional invadopodia—whereas they express some invadopodial markers, they are unable to degrade the ECM.

Interstitial fluid pressure induces changes in the expression of EMT-associated markers

To determine the molecular mechanisms underlying IFP-induced invasive phenotypes, we performed a targeted gene expression analysis over several days of culture using quantitative RT-PCR. We focused on genes associated with epithelial–mesenchymal transition (EMT), a phenotypic switch often implicated in tumor cell invasion.[26] Specifically, we examined the expression of the epithelial markers E-cadherin and keratin-8, and the mesenchymal markers vimentin and Snail. The expression of these genes has previously been shown to be modulated by fluid flow in ovarian cancer cells.[31] Moreover, the invasive response of breast cancer cells to interstitial fluid flow has been shown to vary depending on expression levels of EMT markers.[32]

We found that under interstitial hypotension, which promotes invasion, the expression of vimentin and Snail were significantly elevated over several days compared to other IFP profiles, with the most striking effects observed on days 5 and 6 (Fig. 2). The levels of vimentin and Snail in aggregates subjected to hypertension were not significantly different from the control. Surprisingly, we found that even though hypotension promoted invasion, epithelial genes were significantly upregulated in these aggregates (Fig. 2), and downregulated in those under hypertension. These data suggest that the invasive phenotypes observed under different pressure profiles might result from changes in the expression of genes associated with EMT.
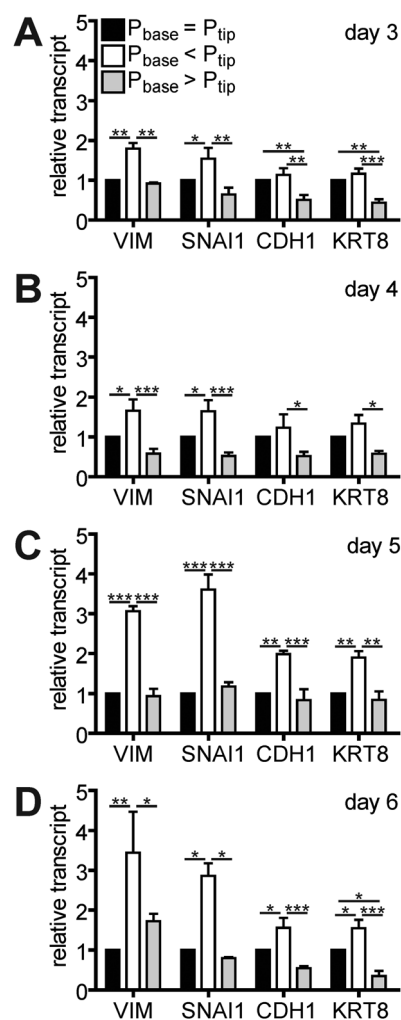

Fig. 2 IFP regulates the expression of EMT markers in human breast cancer aggregates. (A–D) Relative transcript levels of vimentin (VIM), Snail (SNAI1), E-cadherin (CDH1), and keratin-8 (KRT8) in aggregates under $P_{base} = P_{tip}$ ($n = 4$), $P_{base} < P_{tip}$ ($n = 4$), or $P_{base} > P_{tip}$ ($n = 4$) over 3–6 days of culture, respectively. *$P < 0.05$, **$P < 0.01$, ***$P < 0.001$.

Furthermore, elevated expression of mesenchymal and epithelial markers correlate with invasion in this system.

Snail promotes collective invasion and controls invasion length

We next investigated whether the above-described changes in gene expression were required to alter collective invasion in response to IFP. We ectopically expressed Snail by transducing MDA-MB-231 cells with a recombinant adenovirus, resulting in a four-fold increase in Snail, as determined by quantitative RT-PCR (Fig. S3A, ESI†) and immunoblotting analysis (Fig. S3B, ESI†). Ectopic expression of Snail increased the frequency of invasion compared to

control ($P < 0.0001$), even under hypertension, indicating that Snail is sufficient to induce an invasive phenotype (Fig. 3A and B). Snail also increased the number ($P = 0.0003$) (Fig. 3C) and total length ($P < 0.0001$) (Fig. 3D) of multicellular invasions from individual aggregates compared to control. Invadopodia still formed under hypertension in Snail-overexpressing tumor aggregates (Fig. 3B, inset); under hypertension, there was no difference in invadopodial density between AdGFP (1.94 ± 0.13 μm μm^{-1}) and AdSnail (2.06 ± 0.14 μm μm^{-1}) samples.

To determine whether Snail is necessary for invasion in response to IFP, we used an shRNA approach to stably deplete its levels.
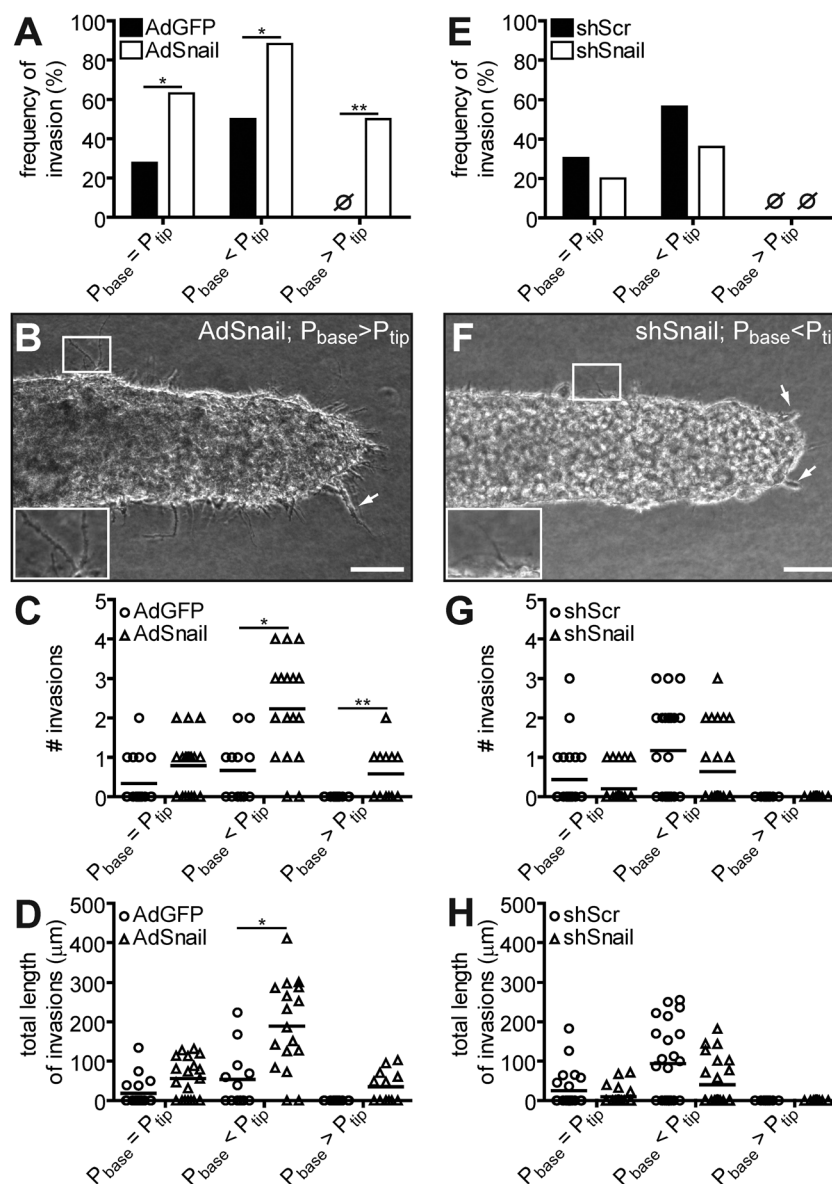

Fig. 3 Snail controls invasion in response to IFP. (A) Frequency of invasion of AdGFP or AdSnail aggregates under $P_{base} = P_{tip}$ (AdGFP: $n = 18$; AdSnail: $n = 19$), $P_{base} < P_{tip}$ (AdGFP: $n = 12$; AdSnail: $n = 17$), or $P_{base} > P_{tip}$ (AdGFP: $n = 16$; AdSnail: $n = 12$). (B) Phase-contrast image of an AdSnail aggregate under $P_{base} > P_{tip}$. Arrow indicates collective invasion. Inset shows magnified image of boxed region. (C) Number and (D) length of invasions in AdGFP or AdSnail aggregates under IFP. (E) Frequency of invasion of shScr or shSnail aggregates under $P_{base} = P_{tip}$ (shScr: $n = 23$; shSnail: $n = 24$), $P_{base} < P_{tip}$ (shScr: $n = 23$; shSnail: $n = 25$), or $P_{base} > P_{tip}$ (shScr: $n = 9$; shSnail: $n = 11$). (F) Phase-contrast image of an shSnail aggregate under $P_{base} < P_{tip}$. Arrows indicate short collective invasion. Inset shows magnified image of boxed region. (G) Number and (H) length of invasions in shScr or shSnail aggregates under IFP. *$P < 0.05$, **$P < 0.01$. Scale bars, 100 μm.

MDA-MB-231 cells were transfected with an shRNA construct targeting Snail (shSnail). The resulting stable cell line showed 75% knockdown of Snail transcript compared to scrambled shRNA control (shScr; Fig. S3C, ESI†), as well as a reduction in Snail protein (Fig. S3D, ESI†). Aggregates expressing shSnail under control pressure or hypotension had a slightly reduced frequency of invasion compared to the shScr control, though differences were not statistically significant (Fig. 3E). Similar to shScr controls, shSnail aggregates did not invade under hypertension. Under hypotension, shSnail aggregates produced short multicellular invasions (Fig. 3F), but invadopodia were still present (Fig. 3F, inset). We observed no difference in invadopodial density between shScr ($2.00 \pm 0.14 \ \mu m \ \mu m^{-1}$) and

shSnail ($1.97 \pm 0.15 \ \mu m \ \mu m^{-1}$) under hypertension, indicating that Snail is not required for invadopodia formation. Furthermore, shSnail did not significantly affect the number of multicellular collective invasions that formed (Fig. 3G), but did decrease their total length ($P = 0.0004$) (Fig. 3H), as compared to control. These results suggest that Snail promotes collective invasion in response to IFP, and may play a role in the lengthening of invasions.

Vimentin is required for collective invasion and formation of invadopodia

We performed a similar series of experiments to examine the role of vimentin in IFP-mediated invasion. Vimentin was expressed
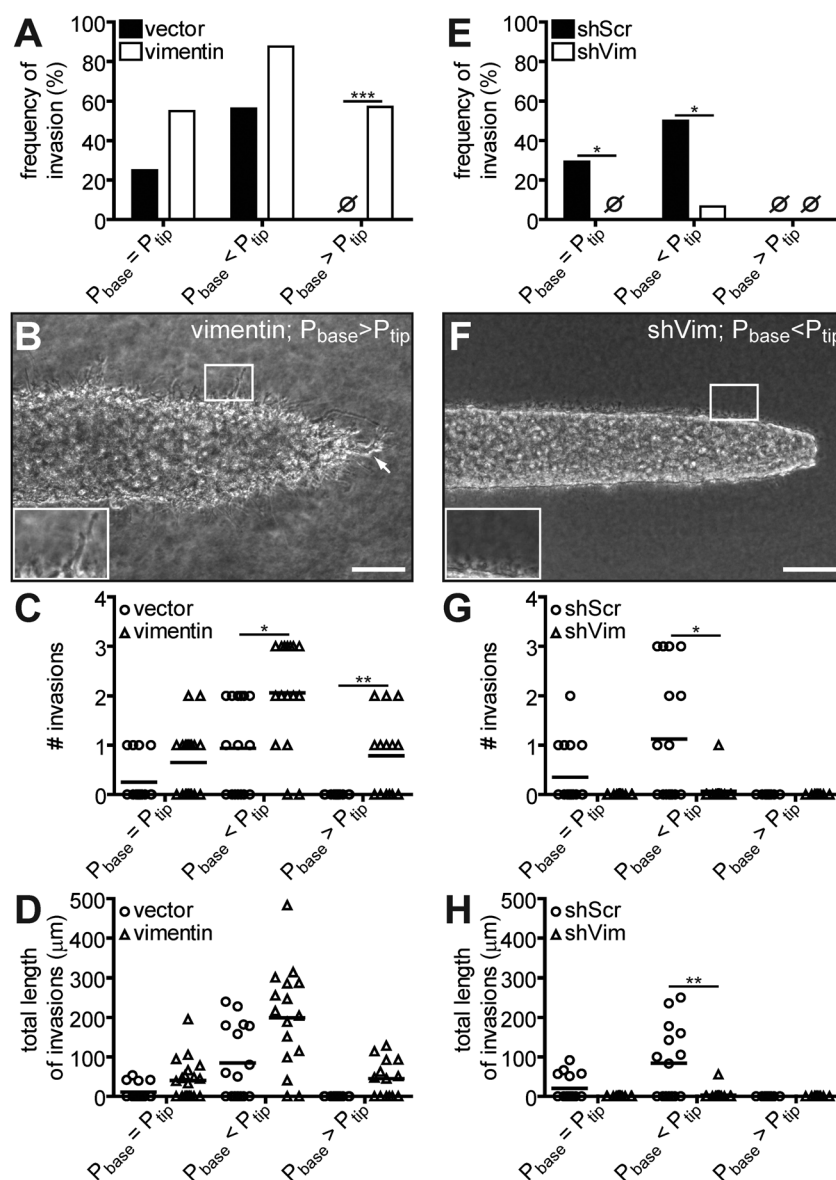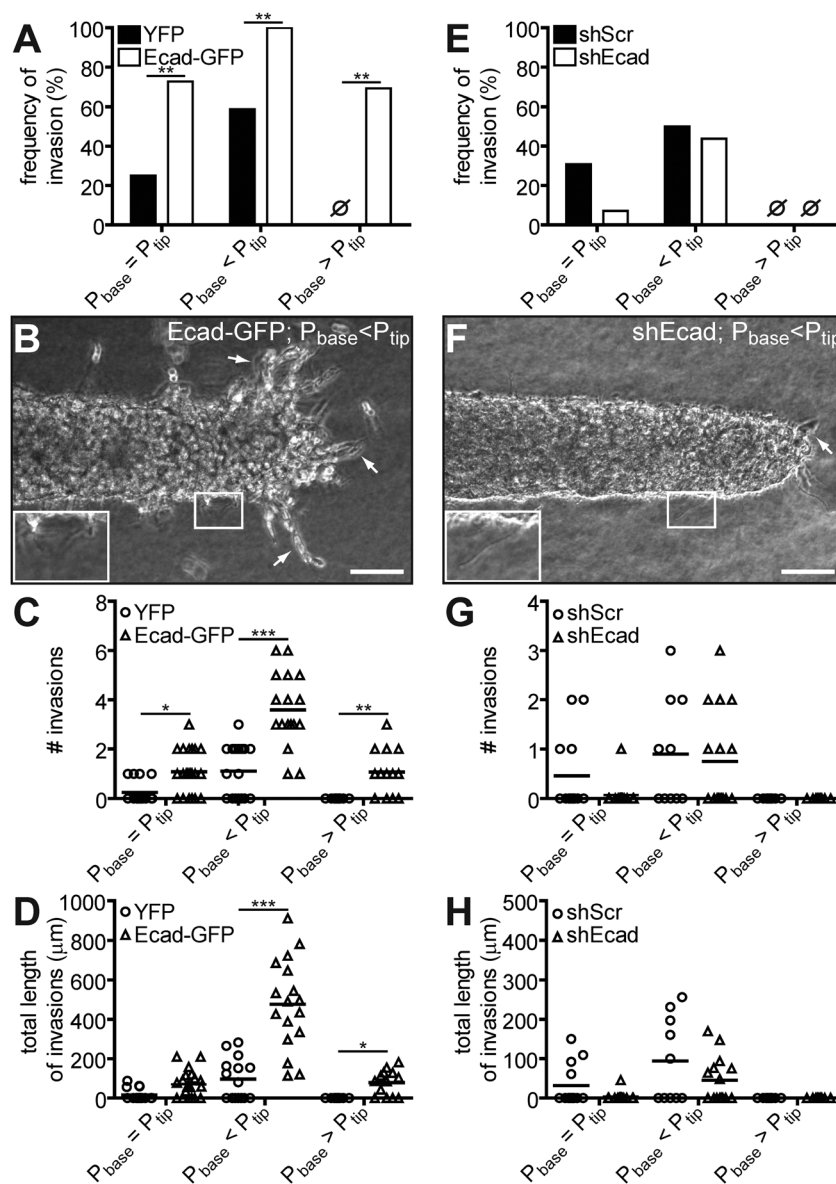

Fig. 4 Vimentin is required for collective invasion in response to IFP. (A) Frequency of invasion of vector or vimentin-expressing aggregates under $P_{base} = P_{tip}$ (vector: $n = 16$; vimentin: $n = 20$), $P_{base} < P_{tip}$ (vector: $n = 16$; vimentin: $n = 16$), or $P_{base} > P_{tip}$ (vector: $n = 15$; vimentin: $n = 14$). (B) Phase-contrast image of a vimentin aggregate under $P_{base} > P_{tip}$. Arrow indicates collective invasion. Inset shows magnified image of boxed region. (C) Number and (D) length of invasions in vector or vimentin aggregates under IFP. (E) Frequency of invasion of shScr or shVim aggregates under $P_{base} = P_{tip}$ (shScr: $n = 16$; shVim: $n = 15$), $P_{base} < P_{tip}$ (shScr: $n = 15$; shVim: $n = 15$), and $P_{base} > P_{tip}$ (shScr: $n = 9$; shVim: $n = 9$). (F) Phase-contrast image of an shVim aggregate under $P_{base} < P_{tip}$. Inset shows magnified image of boxed region. (G) Number and (H) length of invasions in shScr or shVim aggregates under IFP. *$P < 0.05$, **$P < 0.01$, ***$P < 0.001$. Scale bars, 100 μm.

ectopically in MDA-MB-231 cells (Fig. S4A and B, ESI†), which increased the frequency ($P = 0.0002$), number ($P = 0.0007$), and total lengths ($P < 0.0001$) of multicellular collective invasions compared to control (Fig. 4A–D). Ectopic expression of vimentin did not significantly affect invadopodial density (2.17 ± 0.09 μm μm^{-1}) compared to vector control (2.00 ± 0.12 μm μm^{-1}) under hypertension.

To determine whether vimentin expression is necessary for invasion in the engineered tumors, we stably decreased its levels using shRNA (shVim; Fig. S4C and D, ESI†). Depleting vimentin

completely blocked invasion from the shVim aggregates compared to shScr control ($P = 0.0008$) (Fig. 4E), even under hypotension (Fig. 4F–H). These results suggest that vimentin is required for IFP-induced invasion. In addition to inhibiting collective invasion, shVim also inhibited the formation of invadopodia (Fig. 4F, inset). Even under hypertension, invadopodial density was significantly decreased ($P < 0.0001$) in shVim samples (0.40 ± 0.06 μm μm^{-1}) compared to shScr (2.06 ± 0.19 μm μm^{-1}), which is consistent with the prevailing hypothesis that vimentin-containing intermediate filaments are required for the elongation of invadopodia.[33]

Fig. 5 E-cadherin promotes invasion in response to IFP. (A) Frequency of invasion of YFP or Ecad-GFP-expressing aggregates under $P_{base} = P_{tip}$ (YFP: $n = 16$; Ecad-GFP: $n = 22$), $P_{base} < P_{tip}$ (YFP: $n = 17$; Ecad-GFP: $n = 17$), or $P_{base} > P_{tip}$ (YFP: $n = 10$; Ecad-GFP: $n = 13$). (B) Phase-contrast image of an Ecad-GFP aggregate under $P_{base} < P_{tip}$. Arrows indicate collective invasions. Inset shows magnified image of boxed region. (C) Number and (D) length of invasions in YFP or Ecad-GFP aggregates under IFP. (E) Frequency of invasion of shScr or shEcad aggregates under $P_{base} = P_{tip}$ (shScr: $n = 13$; shEcad: $n = 14$), $P_{base} < P_{tip}$ (shScr: $n = 10$; shEcad: $n = 15$), or $P_{base} > P_{tip}$ (shScr: $n = 9$; shEcad: $n = 9$). (F) Phase-contrast image of an shEcad aggregate under $P_{base} < P_{tip}$. Arrow indicates collective invasion. Inset shows magnified image of boxed region. (G) Number and (H) length of invasions in shScr or shEcad aggregates under IFP. *$P < 0.05$, **$P < 0.01$, ***$P < 0.001$. Scale bars, 100 μm.

## E-cadherin promotes extensive collective invasion

Because E-cadherin levels were elevated under hypotension (Fig. 2), which promoted invasion, we hypothesized that E-cadherin-mediated intercellular adhesion might be important for collective invasion under IFP. We created a stable line of MDA-MB-231 cells that expressed elevated levels of an E-cadherin-GFP fusion protein (Ecad-GFP; Fig. S5A and B, ESI†), which surprisingly increased the frequency ($P < 0.0001$), number ($P < 0.0001$), and total lengths ($P < 0.0001$) of invasions compared to control (Fig. 5A–D), and permitted formation of invadopodia (Fig. 5B, inset). There was no difference in invadopodial density between Ecad-GFP ($2.02 \pm 0.11 \ \mu m \ \mu m^{-1}$) and YFP ($2.04 \pm 0.12 \ \mu m \ \mu m^{-1}$) aggregates under hypertension. We observed similar trends in Ecad-GFP-expressing PC-3 aggregates (Fig. S6, ESI†). E-cadherin thus appears to promote collective invasion under IFP.

To determine whether E-cadherin is required for collective invasion, we stably decreased its levels in the aggregates using shRNA (shEcad; Fig. S5C, ESI†). Similar to shSnail, shEcad reduced the frequency of invasion under control pressure or hypotension compared to the shScr control, though these differences were not statistically significant (Fig. 5E). ShEcad aggregates (Fig. 5F) produced a similar number of invasions per aggregate as shScr (Fig. 5G), but the total lengths of invasion per aggregate were shorter ($P = 0.0043$) (Fig. 5H). ShEcad aggregates did not invade under hypertension (Fig. 5E), and invadopodial density was unaffected ($2.09 \pm 0.15 \ \mu m \ \mu m^{-1}$) compared to shScr controls ($2.02 \pm 0.11 \ \mu m \ \mu m^{-1}$). These results suggest that, like Snail, E-cadherin promotes invasion, and may be necessary for extensive collective invasion in response to IFP.

Confocal fluorescence imaging revealed that E-cadherin was diffuse (Fig. 6A and B) and co-localized with β-catenin in Ecad-GFP-expressing aggregates (Fig. S5D, ESI†). No clear cell–cell junctions were discernible, suggesting that transient intercellular contacts may be sufficient for the extensive invasion observed. To determine whether E-cadherin levels *per se* increase ability to invade, we created mosaic aggregates that contained 30% YFP or Ecad-GFP cells. As expected, multicellular invasions from YFP-mosaic aggregates contained ∼30% YFP-expressing cells. In contrast, multicellular invasions from Ecad-GFP-mosaic aggregates (under hypotension) contained ∼96% Ecad-GFP-expressing cells (Fig. 6C). These data suggest that high levels of E-cadherin promote collective invasion in response to IFP, and that invasions are enriched in cells with high levels of E-cadherin. These data may help clarify the clinical finding that breast cancer cells in metastases express higher levels of E-cadherin than those in the primary tumor,[34] by predicting that E-cadherin-overexpressing cells preferentially form initial invasions from the primary site.

## Cells within aggregates are more motile under IFP gradients

IFP regulates the collective invasion of MDA-MB-231 cells from an engineered primary tumor. This finding suggested that IFP might affect the motility of individual cells. We labeled the nuclei of cells in aggregates with H2B-mCherry, and tracked cell positions over 20 hours of culture (Fig. 7A–C). Under hypotension, invading cells migrated farthest from their initial
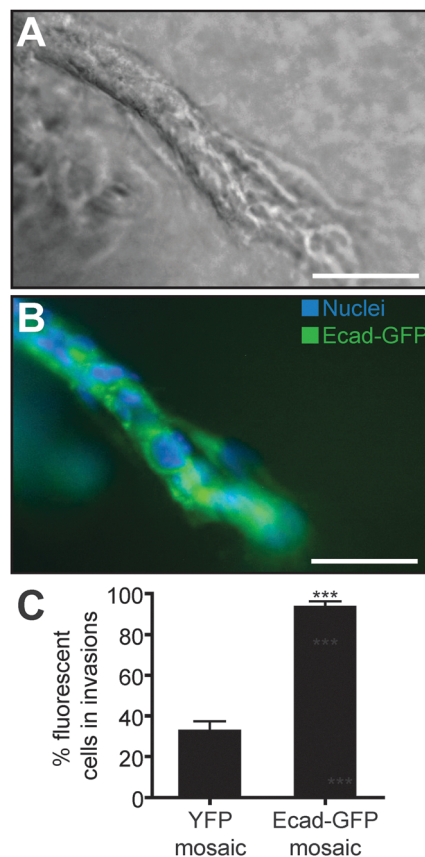
Fig. 6 Cells expressing ectopic E-cadherin preferentially undergo collective invasion. (A) Phase-contrast image of an invasive protrusion from an Ecad-GFP aggregate under $P_{base} < P_{tip}$. (B) Confocal image of the invasion from (A) showing Ecad-GFP localization (green) and Hoechst 33342 staining of cell nuclei (blue). (C) Percentage of fluorescent cells in invasions in aggregates under $P_{base} < P_{tip}$ from YFP or Ecad-GFP mosaic aggregates. ***$P < 0.001$. Scale bars, 50 μm.

positions (Fig. 7B) and against the direction of fluid flow, consistent with recent single-cell suspension studies.[14,15] We also noted that invading cells migrated in a pulsatile fashion, occasionally moving backwards, rather than only progressing forward, congruent with recent observations of collective invasions of normal cells.[25] Cells were also more motile than controls under hypertension (Fig. 7C), despite the fact that these cells did not invade the surrounding ECM. This suggests that gradients in IFP enhance cell motility without necessarily resulting in invasion.

Non-invading cell tracks were used to compute net displacement, path length, and cell speed. Cells in aggregates under hypotension or hypertension migrated further from their starting positions and had longer path lengths than cells under control pressure conditions (Fig. 7D–F). The directionality ratio, a measure of persistence, was higher for cells under hypotension (0.32 ± 0.04) and hypertension (0.27 ± 0.03) compared to the control pressure (0.20 ± 0.03). Cells under IFP gradients also migrated faster; cells under control pressure had an average speed of $3.35 \pm 0.21 \ \mu m \ h^{-1}$ compared to hypotension ($5.80 \pm 0.31 \ \mu m \ h^{-1}$) and hypertension ($5.47 \pm 0.51 \ \mu m \ h^{-1}$). Expression of Ecad-GFP increased net displacement as well as
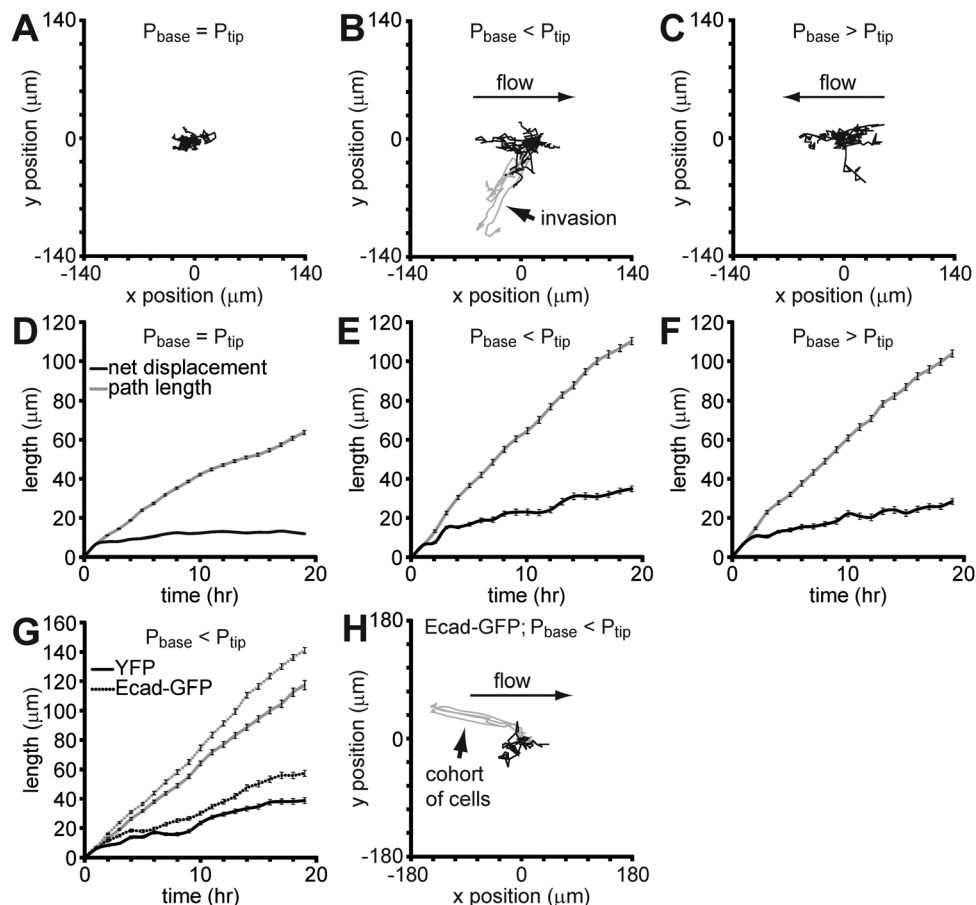
Fig. 7 Cells in aggregates under elevated IFP are motile and persistent. Data are representative of cells in aggregates from three independent experiments. Overlaid individual cell tracks from aggregates under (A) $P_{base} = P_{tip}$ ($n = 16$), (B) $P_{base} < P_{tip}$ ($n = 18$), or (C) $P_{base} > P_{tip}$ ($n = 15$) are shown. Arrows indicate direction of fluid flow. Light grey tracks represent cells undergoing collective invasion. Net displacement (black lines) and path length (grey lines) for non-invading cells in aggregates under (D) $P_{base} = P_{tip}$, (E) $P_{base} < P_{tip}$, and (F) $P_{base} > P_{tip}$. (G) Net displacement (black lines) and path length (grey lines) for YFP (solid lines; $n = 15$) or Ecad-GFP (dotted lines; $n = 21$) cells in aggregates under $P_{base} < P_{tip}$. (H) Overlaid individual cell tracks from non-invading Ecad-GFP cells under $P_{base} < P_{tip}$ ($n = 8$). Light grey tracks indicate cells moving together as a cohort.

path length (Fig. 7G). Ecad-GFP cells also migrated faster (7.43 ± 0.45 μm h^{-1}) than YFP control cells (6.17 ± 0.60 μm h^{-1}). We also noted a subset of non-invading cells within the Ecad-GFP aggregates that migrated together in small groups (2–4 cells) (Fig. 7H). These data suggest that IFP controls collective invasion by modulating the motility of individual cells, in part through E-cadherin.

Discussion

Our data provide molecular insight into how IFP, a physical property of the tumor microenvironment, modulates the collective behavior of tumor cells. We found previously that the direction of IFP-induced flow regulated the invasive phenotype by altering the chemical composition of the interstitial fluid near the surface of the aggregates.[16] Here, we further probed the effects of IFP on invasion by focusing on gene expression and found that the direction of IFP gradients alters the expression levels of the EMT-associated markers Snail, vimentin,

and E-cadherin. Elevated expression of these markers promotes collective invasion, for which vimentin is absolutely required. In addition to affecting the invasive phenotype of multicellular aggregates, IFP also affects the persistence and motility of individual cells, which are regulated by EMT-marker expression. Our system provides insights into the results of single-cell suspension culture models and illuminates how IFP affects collective cell behavior.[13–15,19]

The predominant form of invasion from solid tumors is collective in nature and histological sections of many epithelial tumors reveal collective invasion.[35–37] Our data suggest that cells need not necessarily exhibit a completely mesenchymal phenotype in order to invade collectively from a solid tumor. We observed that aggregates with the highest frequency of collective invasion had elevated levels of both mesenchymal and epithelial markers, and that E-cadherin in particular promoted collective invasion, which suggests an additional role for EMT markers in the cellular response to physical cues such as IFP. These results are consistent with those from other studies showing that E-cadherin expression may actually enhance metastatic potential,[34,38,39]

which contrasts with the classical view of E-cadherin as a tumor suppressor.[40–44] Remarkably, we found that E-cadherin was enriched in invading cohorts. While it is perhaps counter-intuitive for a cell–cell adhesion protein to promote invasion, E-cadherin might permit the directed motion of cohorts by maintaining cohesion between cells.[26] Cell–cell contacts could facilitate the long-range transmission of force, guiding cells in the rear of a cohort to migrate in the same direction as those at the leading edge. We observed this phenomenon in timelapse imaging of Ecad-GFP aggregates; cohorts of cells migrating together had highly correlated motion. Consistently, disrupting adherens junctions was found to impair the directional motion of collectively migrating epithelial cells.[45] Interestingly, however, the localization of E-cadherin in E-cad-GFP invasions was not purely junctional, and E-cadherin appeared to also be present in the cytoplasm. This suggests that aberrant E-cadherin localization might also contribute to increased invasiveness in our system, consistent with previous studies of human breast cancer samples.[34,46] These data support the theory that tumor cells do not need to transition entirely to a mesenchymal cell fate in order to invade from a primary tumor.

In response to IFP, changes in gene expression preceded changes in phenotype, as differences in EMT marker levels persisted over several days prior to invasion. Maintained expression of these proteins may therefore be required to induce downstream signaling for collective invasion in response to IFP. Snail and vimentin are known to interact with key mechano-transduction pathway components: Snail can activate myosin II,[47] and vimentin can activate ERK and protect it from dephosphoryl-ation, in addition to binding to AKT to escape proteolysis.[48–51] Vimentin also plays a role in conferring mechanical stability, protecting cells against compressive stress, as well as enhan-cing their elastic behavior and contractility,[52] which may in turn mediate invasion. In endothelial cells, fluid flow results in rapid translocation of vimentin to the nucleus and near cell–cell junctions,[53] indicating that vimentin is part of the cellular response to physical signals, translating deformations at the cell surface to an intracellular reaction. Consistently, depleting vimentin completely inhibited invasion under all IFP profiles in our system, suggesting that these cells could not respond to IFP. E-cadherin is also involved in the cellular response to mechanical cues via transcriptional regulation.[54] The amplified invasive phenotype of Ecad-GFP aggregates could be related to an enhanced response to IFP. Our data suggest that these EMT markers are required for the translation of physical cues such as IFP into changes in cell behavior.

IFP is known to affect the transport and delivery of cancer therapeutics.[55] Importantly, our results suggest that elevated IFP in vivo, which manifests as interstitial hypertension, also affects cancer cell behavior. Interstitial hypertension may in fact inhibit invasion from the boundary of a primary tumor into the surrounding tissue space. As such, commonly prescribed therapeutics that directly alter IFP may also affect the invasive phenotype of cells in a tumor. Our results also suggest that, within a mechanically heterogeneous tumor, local hypotension could promote cell migration up the pressure gradient.

The main source of interstitial fluid in tumors is the leaky vasculature;[56] tumor cells in close proximity to intratumoral blood vessels, where the local vascular pressure is relatively higher than the interstitial fluid pressure, may be prone to migrate upstream towards these vessels, and potentially metastasize.[15] Determining how IFP contributes to tumor phenotype will be critical for a complete understanding of the interaction between tumor cells and their local microenvironment.

Abbreviations

3D	Three-dimensional
ECM	Extracellular matrix
EMT	Epithelial–mesenchymal transition
IFP	Interstitial fluid pressure
MMP	Matrix metalloproteinase
PDMS	Polydimethylsiloxane

Acknowledgements

References

1 H. J. Burstein, K. Polyak, J. S. Wong, S. C. Lester and C. M. Kaelin, Ductal carcinoma *in situ* of the breast, *N. Engl. J. Med.*, 2004, **350**(14), 1430–1441.

2 S. D. Nathanson and L. Nelson, Interstitial fluid pressure in breast cancer, benign breast conditions, and breast parenchyma, *Ann. Surg. Oncol.*, 1994, **1**(4), 333–338.

3 T. P. Butler, F. H. Grantham and P. M. Gullino, Bulk transfer of fluid in the interstitial compartment of mammary tumors, *Cancer Res.*, 1975, **35**(11 Pt 1), 3084–3088.

4 J. R. Less, M. C. Posner, Y. Boucher, D. Borochovitz, N. Wolmark and R. K. Jain, Interstitial hypertension in human breast and colorectal tumors, *Cancer Res.*, 1992, **52**(22), 6371–6374.

5 Y. Boucher, L. T. Baxter and R. K. Jain, Interstitial pressure gradients in tissue-isolated and subcutaneous tumors: implications for therapy, *Cancer Res.*, 1990, **50**(15), 4478–4484.

6 Y. Boucher, J. M. Kirkwood, D. Opacic, M. Desantis and R. K. Jain, Interstitial hypertension in superficial metastatic

melanomas in humans, *Cancer Res.*, 1991, **51**(24), 6691–6694.

7 R. Gutmann, M. Leunig, J. Feyh, A. E. Goetz, K. Messmer, E. Kastenbauer and R. K. Jain, Interstitial hypertension in head and neck tumors in patients: correlation with tumor size, *Cancer Res.*, 1992, **52**(7), 1993–1995.

8 V. P. Chauhan, T. Stylianopoulos, Y. Boucher and R. K. Jain, Delivery of molecular and nanoscale medicine to tumors: transport barriers and strategies, *Annu. Rev. Chem. Biomol. Eng.*, 2011, **2**, 281–298.

9 T. Hompland, C. Ellingsen, K. M. Ovrebo and E. K. Rofstad, Interstitial fluid pressure and associated lymph node metastasis revealed in tumors by dynamic contrast-enhanced MRI, *Cancer Res.*, 2012, **72**(19), 4899–4908.

10 L. T. Baxter and R. K. Jain, Transport of fluid and macromolecules in tumors. I. Role of interstitial pressure and convection, *Microvasc. Res.*, 1989, **37**(1), 77–104.

11 P. M. Gullino and F. H. Grantham, Studies on the exchange of fluids between host and tumor. I. A method for growing "tissue-isolated" tumors in laboratory animals, *J. Natl. Cancer Inst.*, 1961, **27**, 679–693.

12 M. Milosevic, A. Fyles, D. Hedley, M. Pintilie, W. Levin, L. Manchul and R. Hill, Interstitial fluid pressure predicts survival in patients with cervix cancer independent of clinical prognostic factors and tumor oxygen measurements, *Cancer Res.*, 2001, **61**(17), 6400–6405.

13 U. Haessler, J. C. Teo, D. Foretay, P. Renaud and M. A. Swartz, Migration dynamics of breast cancer cells in a tunable 3D interstitial flow chamber, *Integr. Biol.*, 2012, **4**(4), 401–409.

14 W. J. Polacheck, J. L. Charest and R. D. Kamm, Interstitial flow influences direction of tumor cell migration through competing mechanisms, *Proc. Natl. Acad. Sci. U. S. A.*, 2011, **108**(27), 11115–11120.

15 W. J. Polacheck, A. E. German, A. Mammoto, D. E. Ingber and R. D. Kamm, Mechanotransduction of fluid stresses governs 3D cell migration, *Proc. Natl. Acad. Sci. U. S. A.*, 2014, **111**(7), 2447–2452.

16 J. Tien, J. G. Truslow and C. M. Nelson, Modulation of invasive phenotype by interstitial pressure-driven convection in aggregates of human breast cancer cells, *PLoS One*, 2012, **7**(9), e45191.

17 J. M. Tse, G. Cheng, J. A. Tyrrell, S. A. Wilcox-Adelman, Y. Boucher, R. K. Jain and L. L. Munn, Mechanical compression drives cancer cells toward invasive phenotype, *Proc. Natl. Acad. Sci. U. S. A.*, 2012, **109**(3), 911–916.

18 J. D. Shields, M. E. Fleury, C. Yong, A. A. Tomei, G. J. Randolph and M. A. Swartz, Autologous chemotaxis as a mechanism of tumor cell homing to lymphatics *via* interstitial flow and autocrine CCR7 signaling, *Cancer Cell*, 2007, **11**(6), 526–538.

19 Y. L. Huang, C. K. Tung, A. Zheng, B. J. Kim and M. Wu, Interstitial flows promote amoeboid over mesenchymal motility of breast cancer cells revealed by a three dimensional microfluidic model, *Integr. Biol.*, 2015, **7**(11), 1402–1411.

20 D. W. Infanger, M. E. Lynch and C. Fischbach, Engineered culture models for studies of tumor-microenvironment interactions, *Annu. Rev. Biomed. Eng.*, 2013, **15**, 29–53.

21 J. P. Thiery, H. Acloque, R. Y. Huang and M. A. Nieto, Epithelial–mesenchymal transitions in development and disease, *Cell*, 2009, **139**(5), 871–890.

22 S. R. Chary and R. K. Jain, Direct measurement of interstitial convection and diffusion of albumin in normal and neoplastic tissues by fluorescence photobleaching, *Proc. Natl. Acad. Sci. U. S. A.*, 1989, **86**(14), 5385–5389.

23 K. Lee, Q. K. Chen, C. Lui, M. A. Cichon, D. C. Radisky and C. M. Nelson, Matrix compliance regulates Rac1b localization, NADPH oxidase assembly, and epithelial–mesenchymal transition, *Mol. Biol. Cell*, 2012, **23**(20), 4097–4108.

24 R. Gorelik and A. Gautreau, Quantitative and unbiased analysis of directional persistence in cell migration, *Nat. Protoc.*, 2014, **9**(8), 1931–1943.

25 N. Gjorevski, A. S. Piotrowski, V. D. Varner and C. M. Nelson, Dynamic tensile forces drive collective cell migration through three-dimensional extracellular matrices, *Sci. Rep.*, 2015, **5**, 11458.

26 P. Friedl and D. Gilmour, Collective cell migration in morphogenesis, regeneration and cancer, *Nat. Rev. Mol. Cell Biol.*, 2009, **10**(7), 445–457.

27 P. Friedl, P. B. Noble, P. A. Walton, D. W. Laird, P. J. Chauvin, R. J. Tabah, M. Black and K. S. Zanker, Migration of coordinated cell clusters in mesenchymal and epithelial cancer explants *in vitro*, *Cancer Res.*, 1995, **55**(20), 4557–4560.

28 D. A. Murphy and S. A. Courtneidge, The 'ins' and 'outs' of podosomes and invadopodia: characteristics, formation and function, *Nat. Rev. Mol. Cell Biol.*, 2011, **12**(7), 413–426.

29 A. M. Weaver, Invadopodia: specialized cell structures for cancer invasion, *Clin. Exp. Metastasis*, 2006, **23**(2), 97–105.

30 N. R. Alexander, K. M. Branch, A. Parekh, E. S. Clark, I. C. Iwueke, S. A. Guelcher and A. M. Weaver, Extracellular matrix rigidity promotes invadopodia activity, *Curr. Biol.*, 2008, **18**(17), 1295–1299.

31 I. Rizvi, U. A. Gurkan, S. Tasoglu, N. Alagic, J. P. Celli, L. B. Mensah, Z. Mai, U. Demirci and T. Hasan, Flow induces epithelial–mesenchymal transition, cellular heterogeneity and biomarker modulation in 3D ovarian cancer nodules, *Proc. Natl. Acad. Sci. U. S. A.*, 2013, **110**(22), E1974–E1983.

32 A. M. Tchafa, M. Ta, M. J. Reginato and A. C. Shieh, EMT transition alters interstitial fluid flow-induced signaling in ERBB2-positive breast cancer cells, *Mol. Cancer Res.*, 2015, **189**(3), 541–556.

33 M. Schoumacher, R. D. Goldman, D. Louvard and D. M. Vignjevic, Actin, microtubules, and vimentin intermediate filaments cooperate for elongation of invadopodia, *J. Cell Biol.*, 2010, **189**(3), 541–556.

34 P. J. Kowalski, M. A. Rubin and C. G. Kleer, E-cadherin expression in primary carcinomas of the breast and its distant metastases, *Breast Cancer Res.*, 2003, **5**(6), R217–222.

35 S. Rausch, T. Das, J. R. Soine, T. W. Hofmann, C. H. Boehm, U. S. Schwarz, H. Boehm and J. P. Spatz, Polarizing

cytoskeletal tension to induce leader cell formation during collective cell migration, *Biointerphases*, 2013, **8**(1), 32.

36 H. Mori, N. Gjorevski, J. L. Inman, M. J. Bissell and C. M. Nelson, Self-organization of engineered epithelial tubules by differential cellular motility, *Proc. Natl. Acad. Sci. U. S. A.*, 2009, **106**(35), 14890–14895.

37 X. Trepat, M. R. Wasserman, T. E. Angelini, E. Millet, D. A. Weitz, J. P. Butler and J. J. Fredberg, Physical forces during collective cell migration, *Nat. Phys.*, 2009, **5**(6), 426–430.

38 E. R. Shamir, E. Pappalardo, D. M. Jorgens, K. Coutinho, W. T. Tsai, K. Aziz, M. Auer, P. T. Tran, J. S. Bader and A. J. Ewald, Twist1-induced dissemination preserves epithelial identity and requires E-cadherin, *J. Cell Biol.*, 2014, **204**(5), 839–856.

39 Y. C. Chung, W. C. Wei, S. H. Huang, C. M. Shih, C. P. Hsu, K. J. Chang and W. T. Chao, Rab11 regulates E-cadherin expression and induces cell transformation in colorectal carcinoma, *BMC Cancer*, 2014, **14**, 587.

40 S. Hirohashi, Inactivation of the E-cadherin-mediated cell adhesion system in human cancers, *Am. J. Pathol.*, 1998, **153**(2), 333–339.

41 G. Berx and F. Van Roy, The E-cadherin/catenin complex: an important gatekeeper in breast cancer tumorigenesis and malignant progression, *Breast Cancer Res.*, 2001, **3**(5), 289–293.

42 T. Bogenrieder and M. Herlyn, Axis of evil: molecular mechanisms of cancer metastasis, *Oncogene*, 2003, **22**(42), 6524–6536.

43 P. W. Derksen, X. Liu, F. Saridin, H. van der Gulden, J. Zevenhoven, B. Evers, J. R. van Beijnum, A. W. Griffioen, J. Vink, P. Krimpenfort, J. L. Peterse, R. D. Cardiff, A. Berns and J. Jonkers, Somatic inactivation of E-cadherin and p53 in mice leads to metastatic lobular mammary carcinoma through induction of anoikis resistance and angiogenesis, *Cancer Cell*, 2006, **10**(5), 437–449.

44 J. Yang and R. A. Weinberg, Epithelial–mesenchymal transition: at the crossroads of development and tumor metastasis, *Dev. Cell*, 2008, **14**(6), 818–829.

45 K. E. Worley, D. Shieh and L. Q. Wan, Inhibition of cell–cell adhesion impairs directional epithelial migration on micropatterned surfaces, *Integr. Biol.*, 2015, **7**(5), 580–590.

46 S. A. Rasbridge, C. E. Gillett, S. A. Sampson, F. S. Walsh and R. R. Millis, Epithelial (E-) and placental (P-) cadherin cell adhesion molecule expression in breast carcinoma, *J. Pathol.*, 1993, **169**(2), 245–250.

47 A. C. Martin, M. Gelbart, R. Fernandez-Gonzalez, M. Kaschube and E. F. Wieschaus, Integration of contractile forces during tissue invagination, *J. Cell Biol.*, 2010, **188**(5), 735–749.

48 E. Perlson, I. Michaelevski, N. Kowalsman, K. Ben-Yaakov, M. Shaked, R. Seger, M. Eisenstein and M. Fainzilber, Vimentin binding to phosphorylated Erk sterically hinders enzymatic dephosphorylation of the kinase, *J. Mol. Biol.*, 2006, **364**(5), 938–944.

49 A. Satelli and S. Li, Vimentin in cancer and its potential as a molecular target for cancer therapy, *Cell. Mol. Life Sci.*, 2011, **68**(18), 3033–3046.

50 Q. S. Zhu, K. Rosenblatt, K. L. Huang, G. Lahat, R. Brobey, S. Bolshakov, T. Nguyen, Z. Ding, R. Belousov, K. Bill, X. Luo, A. Lazar, A. Dicker, G. B. Mills, M. C. Hung and D. Lev, Vimentin is a novel AKT1 target mediating motility and invasion, *Oncogene*, 2011, **30**(4), 457–470.

51 R. Virtakoivu, A. Mai, E. Mattila, N. De Franceschi, S. Y. Imanishi, G. Corthals, R. Kaukonen, M. Saari, F. Cheng, E. Torvaldson, V. M. Kosma, A. Mannermaa, G. Muharram, C. Gilles, J. Eriksson, Y. Soini, J. B. Lorens and J. Ivaska, Vimentin-ERK signaling uncouples Slug gene regulatory function, *Cancer Res.*, 2015, **75**(11), 2349–2362.

52 M. G. Mendez, D. Restle and P. A. Janmey, Vimentin enhances cell elastic behavior and protects against compressive stress, *Biophys. J.*, 2014, **107**(2), 314–323.

53 B. P. Helmke, R. D. Goldman and P. F. Davies, Rapid displacement of vimentin intermediate filaments in living endothelial cells exposed to flow, *Circ. Res.*, 2000, **86**(7), 745–752.

54 B. W. Benham-Pyle, B. L. Pruitt and W. J. Nelson, Mechanical strain induces E-cadherin-dependent Yap1 and beta-catenin activation to drive cell cycle entry, *Science*, 2015, **348**(6238), 1024–1027.

55 C. H. Heldin, K. Rubin, K. Pietras and A. Ostman, High interstitial fluid pressure – an obstacle in cancer therapy, *Nat. Rev. Cancer*, 2004, **4**(10), 806–813.

56 Y. Boucher and R. K. Jain, Microvascular pressure is the principal driving force for interstitial hypertension in solid tumors: implications for vascular collapse, *Cancer Res.*, 1992, **52**(18), 5110–5114.

Supplemental Information

Interstitial fluid pressure regulates collective invasion in engineered human breast tumors

via Snail, vimentin, and E-cadherin

Alexandra S. Piotrowski-Daspit, Joe Tien, and Celeste M. Nelson

Supplementary Tables and Figures

Table S1. Primers used for quantitative real-time reverse-transcription PCR (RT-PCR)

| gene	sequences
18S rRNA	Fwd: CGGCGACGACCCATTCGAAC Rev: GAATCGAACCCTGATTCCCCGTC
VIM	Fwd: ATCAACACCGAGTTCAAG Rev: GCCAGCAGGATCTTATTC
SNAI1	Fwd: CCACTCAGATGTCAAGAAG Rev: GCAGGTATGGAGAGGAAG
CDH1	Fwd: CTAATTCTGATTCTGCTGCTCTTG Rev: CCTCTTCTCCGCCTCCTTC
KRT8	Fwd: AGTTACGGTCAACCAGAG Rev: GTCTCCAGCATCTTGTTC
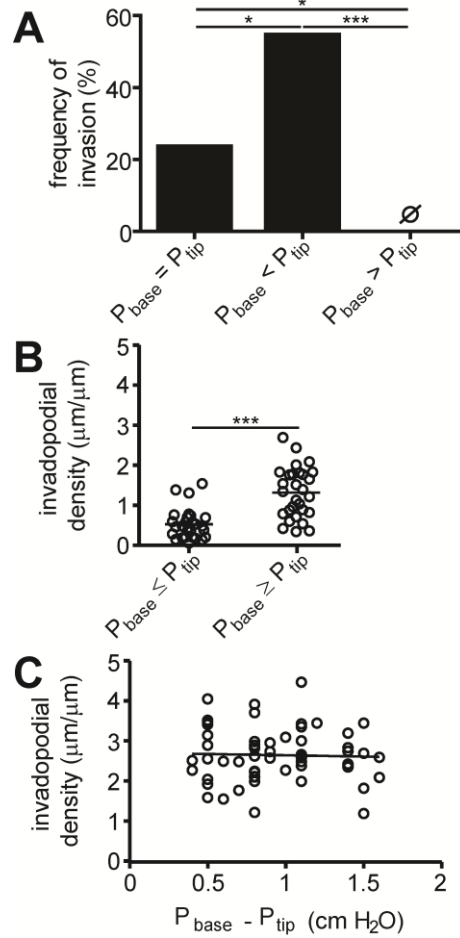
Figure S1. IFP controls invasive phenotype of breast and prostate cancer cells. (**A**) Frequency of invasion of PC-3 cell aggregates under $P_{base}=P_{tip}$ ($n = 27$), $P_{base}<P_{tip}$ ($n = 20$), or $P_{base}>P_{tip}$ ($n = 17$). (**B**) Invadopodial length density for MDA-MB-231 cell aggregates under $P_{base}\leq P_{tip}$ or $P_{base}\geq P_{tip}$. (**C**) Invadopodial density as a function of pressure profile for MDA-MB-231 breast cancer aggregates. The solid line denotes the best least-squares linear fit. * $P<0.05$, ** $P<0.01$, *** $P<0.001$.
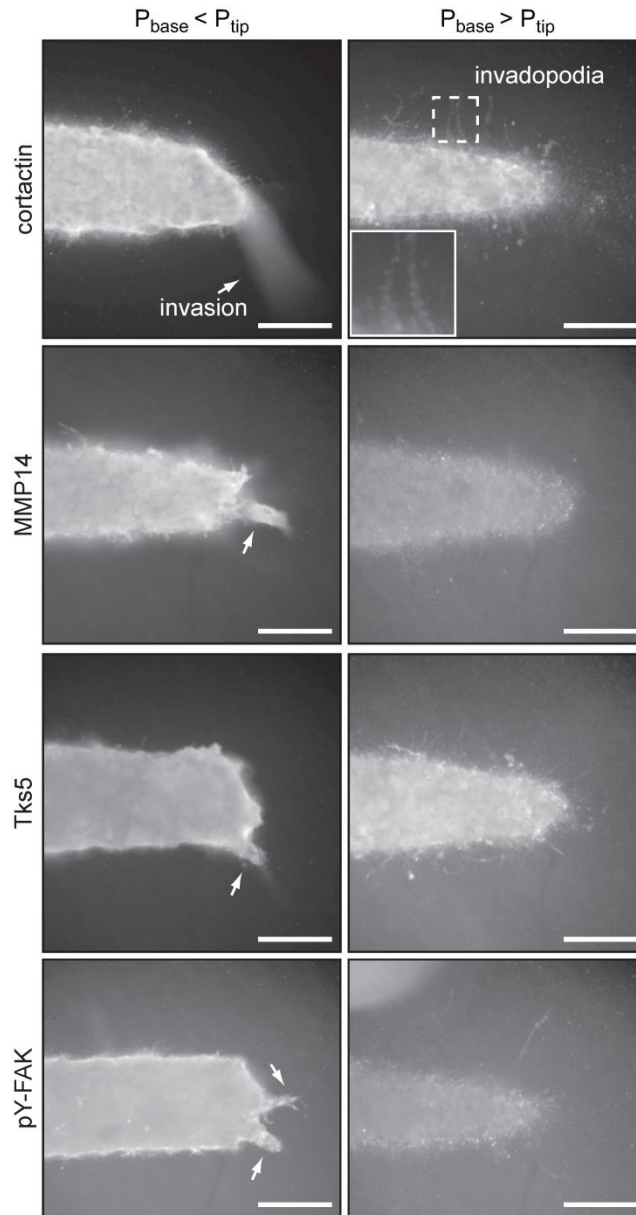
Figure S2. Confocal images of immunofluorescence stains for cortactin, MMP14, Tks5, and phosphorylated FAK (pY-FAK) in MDA-MB-231 cell aggregates under IFP. Arrows denote invasive protrusions containing multiple nuclei; the inset in the right cortactin image magnifies the dotted area. Scale bars, 100 μm.
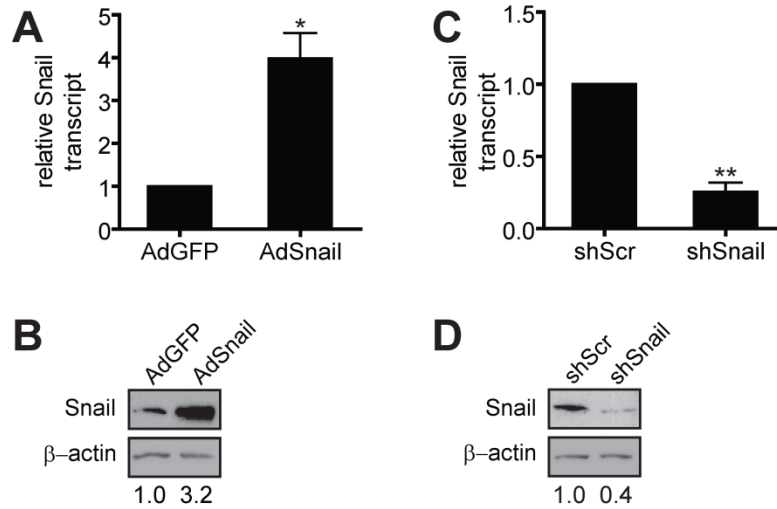
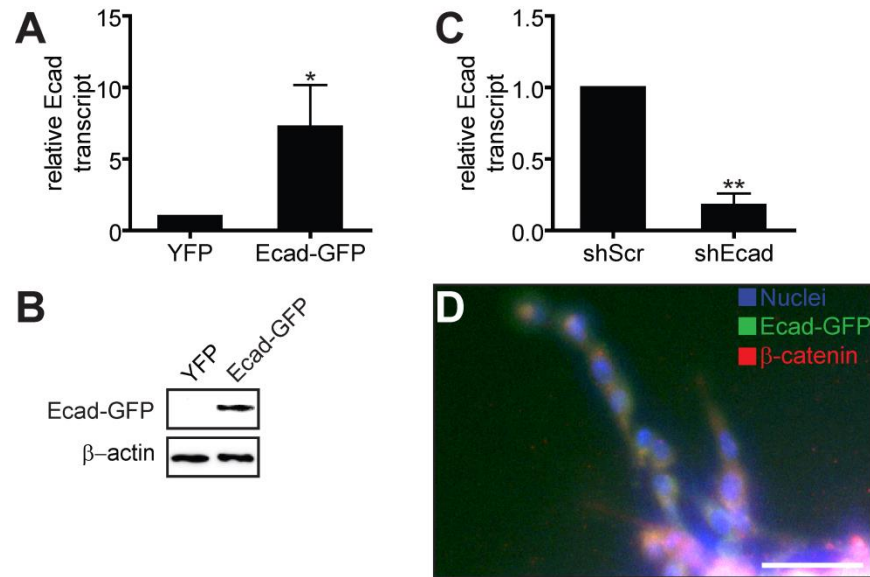**Figure S3.** Snail expression in MDA-MB-231 cells. (**A**) Relative transcript levels of Snail in

AdSnail (*n* = 3) or AdGFP (*n* = 4) MDA-MB-231 cells. (**B**) Immunoblot analysis of MDA-MB-

231 cells transduced with AdGFP or AdSnail. (**C**) Relative transcript levels of Snail in shScr (*n* =

3) or shSnail (*n* = 3) MDA-MB-231 cells. (**D**) Immunoblot analysis for Snail in shScr and

shSnail MDA-MB-231 cells. * $P<0.05$, ** $P<0.01$.
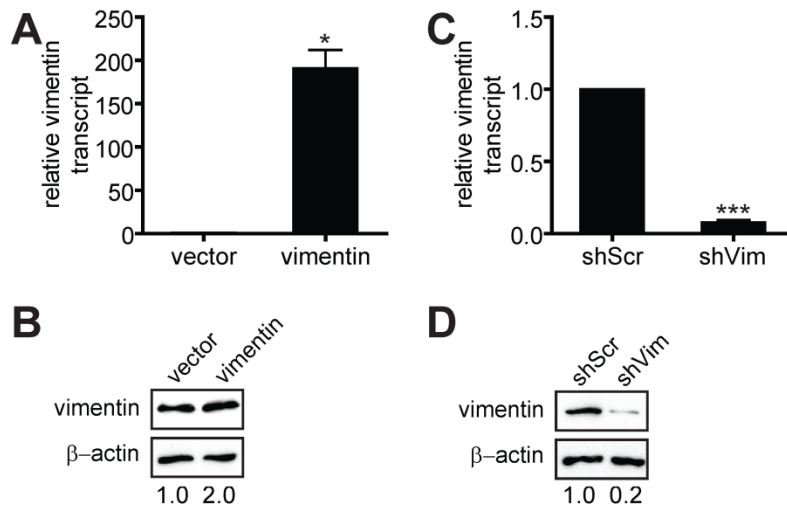
Figure S4. Vimentin expression in MDA-MB-231 cells. (**A**) Relative transcript levels of vimentin in vector ($n = 3$) or vimentin ($n = 3$) MDA-MB-231 cells. (**B**) Immunoblot of vector or vimentin MDA-MB-231 cells. (**C**) Relative transcript levels of vimentin in shScr ($n = 3$) or shVim ($n = 3$) MDA-MB-231 cells. (**D**) Immunoblot analysis for vimentin in shScr or shVim MDA-MB-231 cells. * $P<0.05$, *** $P<0.001$.

Figure S5.

Figure S5. E-cadherin expression in MDA-MB-231 cells. (**A**) Relative transcript levels of E-cadherin in YFP ($n = 3$) or Ecad-GFP ($n = 3$) MDA-MB-231 cells. (**B**) Immunoblot analysis for E-cadherin in YFP or Ecad-GFP MDA-MB-231 cells. (**C**) Relative transcript levels of E-cadherin in shScr ($n = 3$) or shEcad ($n = 3$) MDA-MB-231 cells. (**D**) Immunofluorescence staining for β-catenin (red) and Hoechst 33342 staining of cell nuclei (blue) in invasions from an Ecad-GFP (green) aggregate under $P_{base} < P_{tip}$. * $P < 0.05$, ** $P < 0.01$. Scale bar, 25 μm.
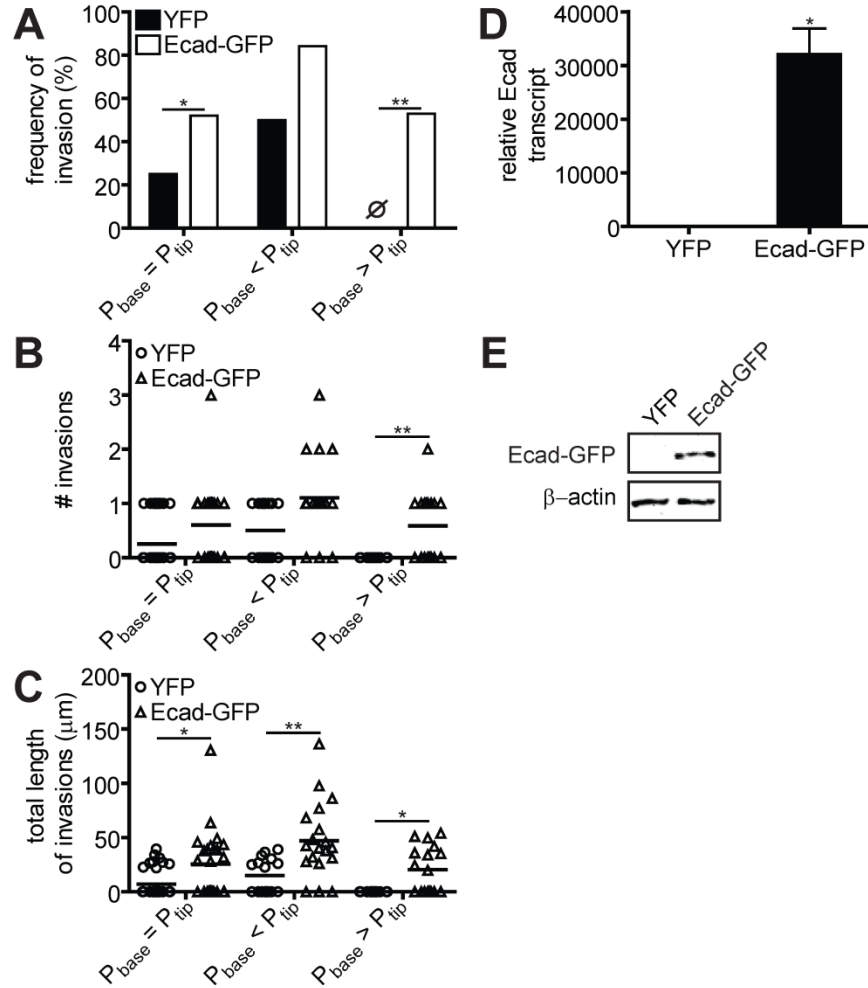
Figure S6.

Figure S6. Ectopic expression of E-cadherin promotes invasion, whereas depletion of E-cadherin inhibits extensive invasion in response to IFP in PC-3 cells. (**A**) Frequency of invasion of YFP or Ecad-GFP-expressing PC-3 aggregates under $P_{base}=P_{tip}$ (YFP: $n = 36$; Ecad-GFP: $n = 25$), $P_{base}<P_{tip}$ (YFP: $n = 16$; Ecad-GFP: $n = 19$), or $P_{base}>P_{tip}$ (YFP: $n = 15$; Ecad-GFP: $n = 17$). (**B**) Number and (**C**) length of invasions in YFP or Ecad-GFP PC-3 aggregates under IFP. (**D**) Relative transcript levels of E-cadherin in YFP ($n = 3$) or Ecad-GFP ($n = 3$) PC-3 cells. (**E**) Immunoblot analysis for E-cadherin in YFP- or Ecad-GFP-transfected PC-3 cells. * $P<0.05$, ** $P<0.01$.